

Efficient estimation of distributional properties of extreme seas from a hierarchical description applied to calculation of un-manning and other weather-related operational windows.

Ross Towe^a, Elena Zanini^a, David Randell^b, Graham Feld^c, Philip Jonathan^{a,d,*}

^aShell Research Limited, London SE1 7NA, United Kingdom.

^bShell Global Solutions International BV, 1031 HW Amsterdam, The Netherlands.

^cShell UK Ltd., Aberdeen AB12 3FY, United Kingdom.

^dDepartment of Mathematics and Statistics, Lancaster University LA1 4YF, United Kingdom.

Abstract

Methods of computational statistics allow efficient estimation of extreme ocean environments, and facilitate optimal operational decision making. We describe estimation of extreme quantiles of total water level and related quantities from a non-stationary hierarchical model for ocean storms. The model incorporates a directional-seasonal extreme value model for occurrences of storm peak significant wave height, a conditional directional model for within-storm evolution of sea states relative to storm peak, a conditional model for the maximum crest within a sea state, and models for total water level. Importance sampling is used for efficient computation of marginal total water level characteristics. We use the model to estimate an optimal un-manning procedure for a notional North Sea offshore structure in severe conditions.

Keywords: hierarchical statistical model; extreme; return value; covariate; importance sampling; weather window; un-manning;

1. Introduction

Quantification of extreme ocean environments is critical to the reliability assessment of offshore and coastal structures. Increasing availability of data from measurements and hindcasts, coupled with easy access to computing resources, has motivated the development of sophisticated methods for statistical characterisation of extreme ocean environments. These methods incorporate the effects of covariates (e.g. direction associated with met-ocean variables such as significant wave height H_S , wind speed and current speed) and extremal dependence (e.g. of extreme significant wave height H_S in space and time, and the dependence between extreme H_S , wind speed and current speed). These approaches also allow uncertainties to be quantified and propagated through design calculations, in principle allowing optimal decision-making (e.g. Jones et al. 2018).

Efficient estimation of extreme ocean environments

Design standards such as NORSOK N-006 (2015), ISO19901-1 (2015), DNVGL-RP-C205 (2017) specify design requirements in terms of return values for met-ocean variables. It is therefore important that models for extreme ocean environments facilitate efficient estimation of return values. The current article provides a description of one such estimation scheme, based on a hierarchical statistical model, in Section 3. For simplicity of description here, the hierarchical model assumes that extreme structural loading results from wave-dominated conditions, and that wave-in-deck is of primary concern. This would be relevant e.g. when sea bed subsidence is thought to occur. That is, the main modelling task is to estimate the distributional characteristics of extreme total water level at a location for return periods of the order of 10^4 years; we emphasise however that the model is easily generalised e.g. to assess reliability with respect to structural loading and utilisation. The distribution of extreme total water level is estimated in terms of (a) a non-stationary directional-seasonal extreme value model for occurrences of storm peak H_S (written H_S^{sp}) assumed to quantify the peaks of independent ocean storms, (b) a conditional model for within-storm evolution of sea state H_S (and related sea state variables) with direction in time relative to H_S^{sp} , and (c) a conditional model for maximum value \tilde{Z} of total water level Z within a sea state with given values of sea state H_S and related variables. The model has been described in previous articles including Randell et al. (2015).

*Corresponding author philip.jonathan@shell.com

The marginal distribution of the annual maximum \tilde{Z}_A of \tilde{Z} (from which return values and related quantities can be calculated) is then estimated by integration over all the conditioning variables, including covariates such as direction and season. This procedure can be computationally expensive; the speed and quality of inference can in general be greatly improved using appropriate sampling techniques such as importance sampling in place of naive Monte Carlo simulation, or numerical integration.

The rationale for un-manning

The various design conditions for an offshore or coastal structure are estimated and re-assessed during the lifetime of the structure. Generally, on design and installation, the structure meets the required design specification; e.g. the return period for wave-in-deck exceeds 10^4 years, or equivalently that the probability that \tilde{Z}_A exceeds the deck height d is less than 10^{-4} . Occasionally, due to effects including (a) improved understanding of the environment and its extremes (e.g. Karpadakis et al. 2019, 2020), (b) improved understanding of physical processes responsible for structural loading (e.g. Schubert et al. 2020, Section 1), (c) changing environment (e.g. Meucci et al. 2020) and (d) changing design requirements (e.g. Feld et al. 2019, Table 1), the structure is found not to be compliant on re-assessment at a later date. That is, $\Pr(\tilde{Z}_A > d) > 10^{-4}$. In this case, mitigating action must be taken to achieve compliance. One approach is to adopt an un-manning strategy for the structure, under which personnel are removed from the structure in certain conditions. Then, for the interval of time per annum for which the structure *is manned* the corresponding annual maximum $\tilde{Z}_A|\text{Manned}$ is such that $\Pr(\tilde{Z}_A|\text{Manned} > d) \leq 10^{-4}$. The un-manning strategy can achieve its ends in principle by a combination of two effects: (a) reduction in the number of manned structural exposure hours per annum regardless of ocean conditions, and (b) un-manning only when ocean conditions are severe. From the safety perspective, and from the economic perspective of maintaining production, it is rational to un-man as infrequently as possible for severe conditions only.

Intuitively, following Hagen and Solland (2009) and related publications (Hagen and Riise 2012, Hagen and Solland 2013 and NORSOK N-006 2015), the met-ocean modeller’s challenge is to establish the highest threshold h^* for sea state H_S at a given location, such that if the structure is un-manned when H_S exceeds h^* , the corresponding manned $\tilde{Z}_A|(H_S < h^*)$ is such that $\Pr(\tilde{Z}_A|(H_S < h^*) > d) \leq 10^{-4}$. Of course, for the un-manning strategy to be useful, knowledge that H_S exceeds h^* is required ahead of time, so that the structure can be un-manned prior to the severe weather arriving. This requires that un-manning is based on forecast sea state \hat{H}_S at the location of interest. The forecast model cannot be perfect; it is uncertain, and in general its uncertainty (quantified e.g. in terms of bias and variance) will increase with forecast lead time. The un-manning challenge must therefore be recast: we seek to establish the highest threshold h^* for *forecast* \hat{H}_S of sea state H_S at a given location, such that if the structure is un-manned when \hat{H}_S exceeds h^* , the corresponding manned $\tilde{Z}_A|(\hat{H}_S < h^*)$ is such that $\Pr(\tilde{Z}_A|(\hat{H}_S < h^*) > d) \leq 10^{-4}$. The estimation of un-manning threshold h^* therefore requires the calculation of the distribution of \tilde{Z}_A restricted to sea states which are forecast not to be too large, so that on the restricted set of sea states (forecast to be less severe), the actual annual probability of wave-in-deck is sufficiently small. This calculation can be performed efficiently using the hierarchical model described above.

Objective and layout

The purpose of this article is to illustrate the efficient estimation of extreme quantiles of met-ocean variables and related quantities, from a non-stationary hierarchical model for extreme ocean environments. We illustrate the estimation scheme in application to the outline specification of an un-manning strategy for a notional offshore platform.

The article is arranged as follows. Section 2 outlines the motivating application and available data. Section 3 then describes the hierarchical model for the ocean environment, focussing on efficient methods for computation of integral properties of interest for un-manning. Section 4 then describes the application of the hierarchical model to estimate optimal un-manning strategies, using the data from Section 2. Section 5 provides discussion and conclusions.

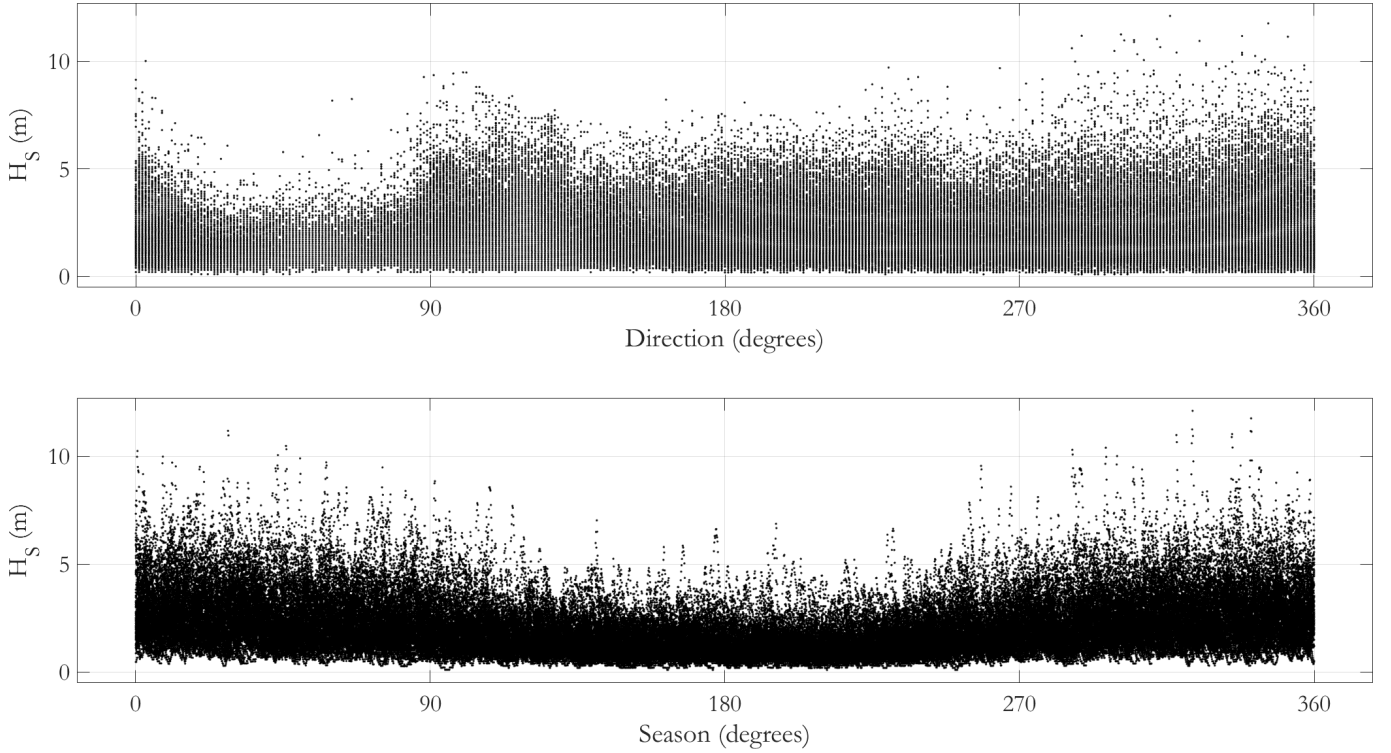


Figure 1: Sea state significant wave height H_S by direction (top) and season (bottom) for the location of interest. Direction is defined clockwise from North in degrees, as the direction from which waves travel. Season is defined as the day of the year projected on to $[0, 360)$ degrees.

2. Motivating application

We use three sources of sea state data in the current work. The first is a historical hindcast of approximately 60 years, used to estimate the hierarchical model for extremes of storm peak H_S^{sp} , sea state H_S and total water level Z . The second and third data sources correspond to 6 years of forecast and measured data used to estimate a calibrated short-term forecast model for sea state H_S , and validate the hindcast, respectively.

Historical hindcast

We use time-series for H_S , (dominant) wave direction, season (defined as day of the year, for a standardised year consisting of 360 days) and related wave period quantities for three hour sea states for the period September 1957 to February 2018 at a northern North Sea location from the hindcast of Reistad et al. (2011). Storm peak characteristics and within-storm trajectories are isolated from these time-series using the procedure described in Ewans and Jonathan (2008). Briefly, contiguous intervals of H_S above a low peak-picking threshold are identified, each interval corresponding to a storm event. The peak-picking threshold corresponds to a directional quantile of H_S with specified non-exceedance probability, estimated using quantile regression. The maximum of significant wave height during the interval is taken as the storm peak significant wave height H_S^{sp} for the storm. The value of other variables at the time of the storm peak significant wave height are referred to as storm peak values of those variables. Consecutive storms within 24 hours of one another are combined. Figure 1 consists of scatter plots of sea state H_S on storm peak direction and season, with direction from which a storm travels expressed in degrees clockwise with respect to north. The effect of fetch limitation with direction is clear e.g. for storms emanating from the north-east. Typical seasonal variation is also present. Note that the development of a hierarchical extreme value model for H_S^{sp} , sea state H_S and total water level Z , using data from the same neighbourhood, has been reported in Feld et al. (2015). For convenience we denote the hindcast data as observations $\{x(t)\}$, $t \in \mathcal{I}_t^{\text{Hnd}}$ of random variables $\{X(t)\}$, where $\mathcal{I}_t^{\text{Hnd}}$ is the period of the hindcast. The hindcast has been shown to provide very good estimates of H_S at locations in the North Sea for which measurements are available. Given this, we consider the hindcast data to be equivalent to measured data for the purposes of this study.

Recent forecast

In addition to historical hindcast data, we also have access to more recent forecast values for sea state H_S for a period of June 2014 to June 2020, referred to as $\mathcal{I}_t^{\text{Clb}}$. For each time point $t \in \mathcal{I}_t^{\text{Clb}}$, the forecast data takes the form

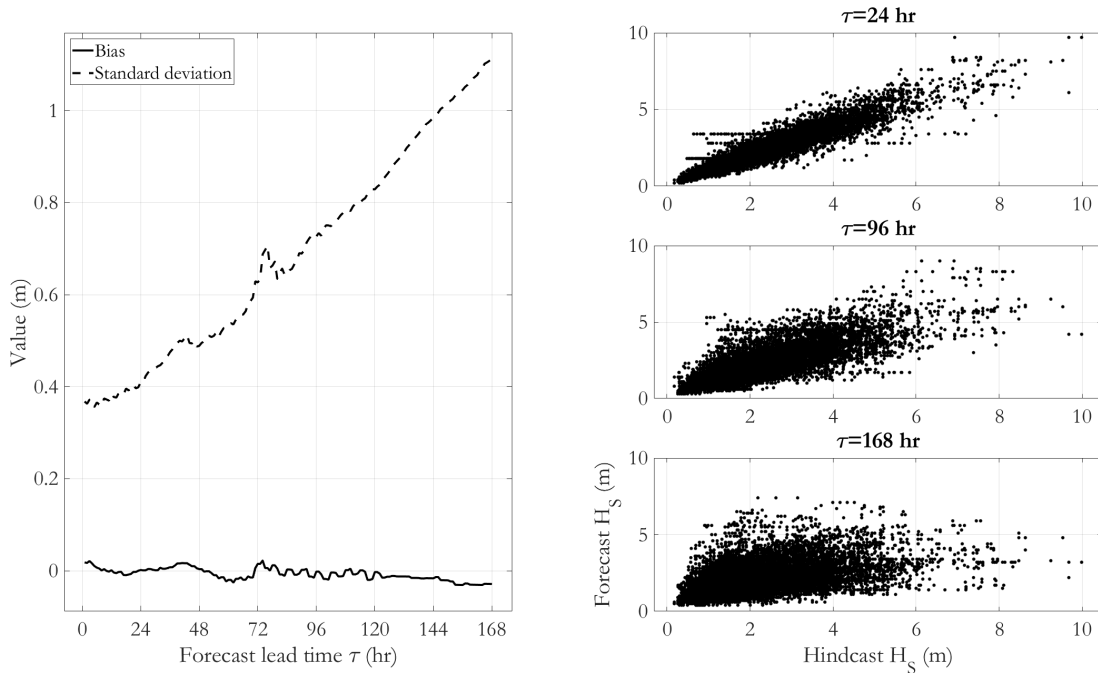


Figure 2: Comparing forecast $(y(\tau; t))$ and hindcast $H_S(x(t + \tau))$ for current time $t \in \mathcal{I}_t^{\text{Clb}} \cap \mathcal{I}_t^{\text{Hnd}}$ and lead time $\tau \in \mathcal{I}_\tau$. Left: bias $E_t[y(\tau; t) - x(t + \tau)]$ and standard deviation $SD_t[y(\tau; t) - x(t + \tau)]$ as a function of forecast lead time τ at current time t . Right: forecast $y(\tau; t)$ for lead times $\tau = 24, 96$ and 168 as a function of hindcast $x(t + \tau)$.

of observations $\{y(\tau; t)\}$ of hourly forecasts $\{Y(\tau; t)\}$ for lead times $\tau \in \mathcal{I}_\tau = \{1, 2, \dots, 7 \times 24\}$ with a maximum lead time of 7 days. Any missing hourly values in the forecast were imputed by interpolation. The left panel of Figure 2 illustrates forecast performance in terms of estimated bias $E_t[Y(\tau; t) - X(t + \tau)]$ and estimated standard deviation $SD_t[Y(\tau; t) - X(t + \tau)]$ as a function of lead time τ , for $t \in \mathcal{I}_t^{\text{Clb}} \cap \mathcal{I}_t^{\text{Hnd}}$. The right panels of Figure 2 gives scatter plots of the forecast $y(\tau; t)$ on the hindcast $x(t + \tau)$ for $\tau = 24, 96$ and 168 . As might be expected, the left panel suggests that the forecast is approximately unbiased for all lead times τ , but its uncertainty increases with τ . There is also evidence from the right panel that the extent of bias changes with the forecast value, especially for larger τ . Specifically, it appears that, when τ is large, the forecast tends to underestimate the largest values of H_S at the location under consideration. This in turn suggests some potential to estimate an improved calibrated forecast for this location, explored further in Section 4.1.

3. Efficient estimation of optimal un-manning

3.1. The hierarchical model

The hierarchical model has a number of components as noted in the introduction, involving the characterisation of (a) storm peak H_S^{sp} using non-stationary extreme value analysis, (b) non-stationary within-storm evolution of H_S (and related quantities) relative to H_S^{sp} , and (c) the estimation of the distribution of sea state maximum total water level \tilde{Z} given sea state H_S and related quantities. Here, we describe the hierarchical model qualitatively, referring the reader to previous articles including Randell et al. (2015) for a fuller mathematical description.

The model assumes that occurrences of severe ocean storms, and hence of storm peak H_S^{sp} , can be considered to be approximately independent in time, and that the magnitudes of exceedances of storm peak H_S^{sp} over a high threshold given covariates follow a generalised Pareto distribution. These assumptions are demonstrated to be reasonable during application using e.g. diagnostic plots. Given these assumptions, the specification of the full hierarchical model for total water level (composed of elements (a), (b) and (c) here) is relatively straightforward.

3.1.1. Storm peaks

The non-stationary model for H_S^{sp} as a function of one or more covariates itself involves three steps: (i) a quantile regression model for extreme value threshold estimation yielding threshold ψ corresponding to non-exceedance probability γ , for values of γ on some interval $\mathcal{I}_\gamma \in (0, 1)$, (ii) a Poisson model for the rate of occurrence of threshold exceedance yielding rate ρ , and (iii) a generalised Pareto model for the size of threshold exceedance, characterised in terms of a shape parameter ξ and scale parameter σ . We therefore estimate uncertain, non-stationary estimates for a

total of four quantities, written together as $\eta = \{\psi, \rho, \sigma, \xi\}$ such that $\eta_1 = \psi$, $\eta_2 = \rho$, etc. Note that all element of η vary with covariates (such as season and direction) and extreme value threshold γ .

Each of models (i-iii) is estimated using a spline representation of model parameter variation with covariate on a set of combinations of covariate values as discussed in e.g. Randell et al. (2015) and Zanini et al. (2020) on full directional-seasonal covariate domain $\mathcal{P} = [0, 360) \times [0, 360)$. For example, we might estimate a directional-seasonal model for each point d on a regular 2-D lattice of 32 directions (with spacing 11.25°), and 24 seasonal points (with spacing of 15 seasonal degrees, corresponding to approximately 2 weeks) yielding an index set \mathcal{I}_d with $32 \times 24 = 768$ members.

The uncertainty of estimated model parameters can be quantified using a bootstrapping scheme in which the whole analysis (a) is repeated for multiple independent bootstrap resamples $b \in \mathcal{I}_b$ of the original H_S^{sp} sample. Note that uncertainty regarding the choice of non-exceedance probability γ can also be incorporated at this stage, so that a given value of γ is associated with each bootstrap resample b . We can therefore write the set of estimates generated by analysis (a) as $\{\eta_{jdb}\}$, $j \in \mathcal{I}_j = \{1, 2, 3, 4\}$, $d \in \mathcal{I}_d$ and $b \in \mathcal{I}_b$. Thus the array of estimates $\eta_{\bullet\bullet b}$ fully characterises the non-stationary extreme value model corresponding to bootstrap resample b .

Informally in more mathematical notation, the quantile regression and Poisson models (i-ii) are used to construct an estimate for the conditional joint distribution $\Theta^*, \Phi^* | \mathcal{B}$ of peak direction Θ^* and season Φ^* for a storm, given bootstrap sample \mathcal{B} . They also provide an estimate for $R | \mathcal{B}$, the *omni-covariate* annual rate of occurrence of storms given \mathcal{B} . The quantile regression and generalised Pareto model provide an estimate for the conditional distribution $X^* | \Theta^*, \Phi^*, \mathcal{B}$ of storm peak exceedances X^* given storm peak direction, season and bootstrap sample. These estimates for distributions of storm peak characteristics contribute to the estimation of the annual distribution of maximum total water level in Section 3.2.

3.1.2. Within-storm evolution of sea states

Estimating the evolution of H_S (and related quantities; (b) above) in time and direction relative to H_S^{sp} using a simple statistical model is challenging (but see e.g. Tendijck et al. 2019). For this reason, we adopt an empirical approach using a look-up table. Simply, we isolate historical storm trajectories with similar given storm peak characteristics, and use this sample of trajectories (potentially adjusted to maintain some conditions such as peak direction, peak season and peak steepness) as an empirical description of the joint conditional distribution of sea state H_S (and related quantities) given those storm peak characteristics. This has proven a useful pragmatic approach, especially for simulation of joint evolution of sea state variables using the hierarchical model. The approach gives a means to sample from the joint distribution $\{X_s, \Theta_s, \Phi_s, \Omega_s\} | X^*, \Theta^*, \Phi^*$ of the (time series) of sea state H_S (X_s), storm direction Θ_s , season Φ_s and other variables Ω_s given storm peak characteristics X^*, Θ^* and Φ^* for each of $s \in \mathcal{S}$ sea states of the storm, exploited in Section 3.2. The vector Ω_s contains all other sea-state variables needed for the analysis, and might (e.g.) include spectral information for the sea state, or surge and seasonal tide.

3.1.3. Maximum total water level within a sea state

Finally, the conditional distribution of total water level Z (and hence of maximum total water level \tilde{Z} in a sea state; (c) above) is taken to follow the parametric form of Forristall (2000) for maximum crest, with corrections as appropriate for sea state surge and tide. This provides an estimate for the distribution $\tilde{Z}_s | X_s, \Theta_s, \Phi_s, \Omega_s$ of maximum total water level given sea state H_S , direction, season and other variables, also used in Section 3.2. Note that a number of other distributional forms for maximum crest are available.

In more general applications of the hierarchical model, we might consider replacing maximum total water level within a sea state with some other variable related to structural loading or utilisation of an offshore structure. In this sense, maximum total water level can be viewed as the “response” of interest in the current work.

3.2. The annual distribution of maximum total water level

Using the hierarchical model, the annual distribution of the maximum total water level \tilde{Z} over all sea states and storms can be expressed in terms of the distributions estimated in Section 3.1. For clarity we present the result first in terms of the distribution of maximum total water level within a storm.

3.2.1. The distribution of maximum total water level within a storm

Integration over the distributions introduced in Section 3.1 gives

$$\begin{aligned}
F_{\tilde{Z}|\mathcal{B}}(z|b) &= \int_{\phi^*} \int_{\theta^*} \int_{x^*} \int_{\{x_s, \theta_s, \phi_s, \omega_s\}} \left[\prod_{s \in \mathcal{S}|X^*, \Theta^*, \Phi^*} F_{\tilde{Z}_s|X_s, \Theta_s, \Phi_s, \Omega_s}(z|x_s, \theta_s, \phi_s, \omega_s) \right] \\
&\times f_{\{X_s, \Theta_s, \Phi_s, \Omega_s\}|X^*, \Theta^*, \Phi^*}(\{x_s, \theta_s, \phi_s, \omega_s\}|x^*, \theta^*, \phi^*) \\
&\times f_{X^*|\Theta^*, \Phi^*, \mathcal{B}}(x^*|\theta^*, \phi^*, b) \\
&\times f_{\Theta^*, \Phi^*|\mathcal{B}}(\theta^*, \phi^*|b) d\{x_s, \theta_s, \phi_s, \omega_s\} dx^* d\theta^* d\phi^* \tag{1}
\end{aligned}$$

for bootstrap resample b . The integrand involves the storm distribution of peak direction and season, the conditional distribution of H_S^{sp} given storm peak direction and season, the joint distribution of sea state H_S , direction and season (for all sea states $s \in \mathcal{S}$ in the storm) given storm peak characteristics, and finally distribution of maximum total water level in each of the sea states given sea state characteristics. The integral is taken over all sea state variables (for all sea states in the storm), and over all storm peak variables. The result is the distribution of maximum total water level \tilde{Z} on the full covariate domain \mathcal{P} given bootstrap resample b .

3.3. Optimal un-manning

As motivated in Section 1, un-manning can be appropriate for offshore structures which, when manned throughout the year, do not satisfy safety conditions. The objective of optimal un-manning is to un-man the structure as infrequently as possible, in such a way that when manned, the structure satisfies the required safety condition. Otherwise when un-manned, the structures would need to comply with less stringent regulatory requirements for un-manned structures. It is logical, based on safety considerations, to un-man for time periods corresponding to severe environments; therefore, the optimal un-manning strategy must be based on forecasts of upcoming severe events. In the current work, we focus on wave-in-deck as the condition of interest, and assume that the safety condition takes the form $\Pr(\tilde{Z}_A|\text{Manned} > d) \leq \delta$, where \tilde{Z}_A is the annual maximum total water level, d is the deck height and δ is the appropriate threshold probability, assumed to be $\delta = 10^{-4}$ here; this corresponds to a return period $T = 1/\delta = 10^4$ years. More formally therefore, optimal un-manning seeks to establish the highest threshold h^* for forecast \hat{H}_S of sea state H_S at the location of interest, such that if the structure is un-manned when \hat{H}_S exceeds h^* , the corresponding manned maximum annual total water level distribution is such that $\Pr(\tilde{Z}_A|(\hat{H}_S < h^*) > d) \leq \delta$.

3.3.1. Integral for un-manning

Adopting the notation of Section 3.1, with Y referring to a specific forecast \hat{H}_S of any sea state H_S , for example using a particular combination of forecast model and lead time τ , optimal un-manning seeks h^* such that

$$h^* = \operatorname{argmax}_h \left[F_{\tilde{Z}_A|Y \leq h}(d|h) \geq (1 - \delta) \right] \tag{2}$$

for return period $T = 1/\delta$ years and deck height d , where $F_{\tilde{Z}_A|Y \leq h}$ is the distribution of annual maximum total water level, restricted to cases where forecast H_S does not exceed h . For any bootstrap resample b , the conditional distribution function of $\tilde{Z}_A|Y \leq h, \mathcal{B}$ can be derived directly by adapting Equation 1, as

$$\begin{aligned}
F_{\tilde{Z}|Y \leq h, \mathcal{B}}(z|h, b) &= \int_{\phi^*} \int_{\theta^*} \int_{x^*} \int_{\{x_s, \theta_s, \phi_s, \omega_s\}} \\
&\left[\prod_{s \in \mathcal{S}|X^*, \Theta^*, \Phi^*} F_{\tilde{Z}_s|X_s, \Theta_s, \Phi_s, \Omega_s}(z|x_s, \theta_s, \phi_s, \omega_s)^{\mathbb{I}(Y_s \leq h)} \right] \\
&\times f_{\{X_s, \Theta_s, \Phi_s, \Omega_s\}|X^*, \Theta^*, \Phi^*}(\{x_s, \theta_s, \phi_s, \omega_s\}|x^*, \theta^*, \phi^*) \\
&\times f_{X^*|\Theta^*, \Phi^*, \mathcal{B}}(x^*|\theta^*, \phi^*, b) \\
&\times f_{\Theta^*, \Phi^*|\mathcal{B}}(\theta^*, \phi^*|b) d\{x_s, \theta_s, \phi_s, \omega_s\} dx^* d\theta^* d\phi^* \tag{3}
\end{aligned}$$

where Y_s refers to the forecast H_S for storm sea state $s \in \mathcal{S}$. The indicator function \mathbb{I} returns zero if its argument is false, and unity otherwise. Hence the exponent term $\mathbb{I}(Y_s < h)$ only admits sea states for which forecast H_S does not exceed h ; this is the basis of the un-manning calculation.

3.3.2. The distribution of the annual maximum total water level

Using Equation 4, the distribution of the annual maximum total water level $\tilde{Z}_A|Y \leq h, \mathcal{B}$ can now be calculated as

$$F_{\tilde{Z}_A|Y \leq h, \mathcal{B}}(z|h, b) = \exp[-\lambda(b)(1 - F_{\tilde{Z}|Y \leq h, \mathcal{B}}(z|h, b))] \quad (5)$$

where $\lambda(b)$ is the *omni-covariate* annual rate of occurrence of storms for bootstrap resample b . The bootstrap average (predictive) distribution of annual maximum total water level on the full covariate domain \mathcal{P} is then simply estimated as

$$F_{\tilde{Z}_A|Y \leq h}(z|h) = \frac{1}{n_b} \sum_{b \in \mathcal{I}_b} F_{\tilde{Z}_A|Y \leq h, \mathcal{B}}(z|h, b) \quad (6)$$

where n_b ($= |\mathcal{I}_b|$) is the number of bootstrap resamples. Expression 6 incorporates all the covariate variation in storm peaks and in storm evolution, as well as sampling uncertainty, in the estimated distribution $F_{\tilde{Z}_A|Y \leq h}$, in a principled manner. Using Equations 5, 6 and 2 we can then estimate the optimal un-manning threshold h^* . By further restricting the calculation in Equation 4 to some subdomain $\mathcal{P}' \subseteq \mathcal{P}$ (i.e. by replacing the exponent $\mathbb{I}(Y_s \leq h)$ by $\mathbb{I}(((\theta_s, \phi_s) \in \mathcal{P}') \cap (Y_s \leq h))$), the distribution $\tilde{Z}|\mathcal{P}', Y \leq h, \mathcal{B}$ of annual (restricted) maximum total water level in a storm for covariate subdomain \mathcal{P}' can also be evaluated (interesting e.g. for calculation of directional and seasonal design and un-manning criteria).

3.3.3. A predictive model for forecast H_S using the hindcast

The hierarchical model fitted to hindcast data provides a means to estimate all the distributions required to evaluate the integral in Equation 4. However, we also need to know the forecast Y corresponding to any sea state of any possible storm. Unfortunately, this data is not available as part of the hindcast. Instead, for the time period over which forecast and hindcast data are available, we estimate a simple statistical model for the Y as a functions of X .

In the notation of Section 2, for the time period $t \in \mathcal{I}_t^{\text{Clib}} \cap \mathcal{I}_t^{\text{Hnd}}$ over which both forecast and hindcast data are available, we assume that the forecast $Y(\tau; t)$ at lead time $\tau \in \mathcal{I}_\tau$ is related to the hindcast value $X(t + \tau)$ by

$$Y(\tau; t)|(X(t + \tau) = x) = \alpha(\tau) + \beta(\tau)x + \epsilon\sigma(\tau) \quad (7)$$

with intercept α , slope β and error standard deviation σ , where ϵ is a random variable from a standard Gaussian distribution, drawn independently for any t and τ . All of α , β and σ are functions of lead time τ , but independent of t . We expect that forecast variability increases with lead time, and hence that $\sigma(\tau)$ is an increasing function. Similarly, we expect good agreement between $Y(\tau; t)$ and $X(t + \tau)$ for small τ ; hence the value of $\beta(\tau)$ should be near unity here, and the corresponding value of $\alpha(\tau)$ near zero. With increasing τ , the value of $\beta(\tau)$ reduces, with a compensatory increase in $\alpha(\tau)$ required to maintain the mean value of forecast H_S . Illustrations of fitted models for the North Sea application are given in Section 4.1. Using the model in Equation 7 in the un-manning calculation outlined in Section 3.3.1, we are able to estimate the optimal un-manning threshold h^* for each lead time τ of interest.

3.4. Efficient integration

The integral in Equation 4 is computationally challenging to evaluate. Moreover, solution of Equation 2 requires repeated evaluation of the integral in Equation 4 for different choices of h . Efficient evaluation of integrals such as those in Equations 4 and 1 is clearly therefore of some relevance. In this section we describe two approaches to achieve this. The first approach, based on straightforward Monte Carlo sampling, is conceptually easier to understand but computationally inefficient. The second computationally-efficient approach based on importance sampling is used in practice.

3.4.1. Monte Carlo sampling

The most intuitively obvious approach to evaluation of the integral in Equation 4 is Monte Carlo sampling. The calculation is straightforward but laborious. We choose to summarise it as Algorithm 1, the steps of which mirror sampling from the different distributions in the calculation described by Equation 4.

The procedure in Algorithm 1 can be refined when interest lies in specific covariate subdomains, such as all-season directional octants. However, to estimate the tail of the distribution of $\tilde{Z}_A|Y < h$ well, this simple Monte Carlo scheme would need to sample the tail region sufficiently frequently. For small return periods T , this is generally not an issue; hence Monte Carlo works relatively well. However, for large T , a large number of Monte Carlo iterations would be necessary. For example, to sample 100 values from the tail at approximately 10^4 -year level, we need to simulate 10^6 years of observations. For this reason, more computationally-efficient approaches are needed.

Input: Estimated extreme value models for bootstrap resamples indexed by $b \in \mathcal{I}_b$ for set of non-exceedance probabilities $\gamma \in \mathcal{I}_\gamma$, set of forecast H_S thresholds $h \in \mathcal{I}_h$;

- 1 **for** each h in \mathcal{I}_h **do**
- 2 **for** each b in \mathcal{I}_b **do**
- 3 **for** $i = 1, 2, \dots$ Monte Carlo iterations **do**
- 4 Sample storm peak direction θ^* and season ϕ^* from the estimated Poisson model (ii) for the rate of occurrence of storm peak events exceeding threshold ψ for non-exceedance probability γ ;
- 5 Sample H_S^{sp} value x^* from the estimated generalised Pareto (iii) model for H_S^{sp} ;
- 6 Select and adjust a historical storm trajectory that provides a good empirical match (based on some measure of distance of historical storm peak to sampled x^* , θ^* and ϕ^* ; see Section 3.1.2). This provides a time series of $\{x_s, \theta_s, \phi_s, \omega_s\}$ for $s \in \mathcal{S}$, and is equivalent to sampling from the joint distribution $\{X_s, \Theta_s, \Phi_s, \Omega_s\} | X^*, \Theta^*, \Phi^*$;
- 7 For each sea state s in the storm, sample maximum total water level c_s (Section 3.1.3);
- 8 For each sea state s in the storm, sample forecast H_S value y_s using x_s for lead time τ using the regression model in Equation 7;
- 9 Identify those sea states for which forecast H_S is such that $y_s < h$;
- 10 Estimate the maximum total water level $\tilde{z}_i = \max_{s | Y_s < h} \{c_s\}$. Retain \tilde{z}_i as a sample from the distribution of $\tilde{Z} | Y < h, b$ for iteration i , for the given γ and h ;
- 11 **end**
- 12 Accumulate the empirical distribution $F_{\tilde{Z} | Y < h, \mathcal{B}}(z | h, b)$;
- 13 **end**
- 14 Estimate the bootstrap-average distribution $F_{\tilde{Z} | Y < h}(z | h)$ of restricted annual maximum total water level using Equations 5 and 6;
- 15 **end**
- 16 Identify the un-manning threshold h^* using Equation 2;

Output: Optimal un-manning threshold h^*

Algorithm 1: Monte Carlo sampling algorithm for estimation of un-manning threshold.

3.4.2. Importance sampling

When return period T is large, importance sampling (e.g. Gelfand 1994, Davison 2003, Northrop et al. 2017) is more efficient than simple Monte Carlo: importance sampling reduces the uncertainty in estimation of the distribution of $\tilde{Z}_A|Y \leq h$ relative to Monte Carlo sampling (from a similar number of samples).

The motivation for importance sampling is that certain values of the random variables $X^*, \Theta^*, \Phi^*, \{X, \Theta_s, \Phi_s\}$ have more impact on the estimation of the distribution of $\tilde{Z}_A|Y \leq h$ than others. Specifically, extreme values of X^* are likely to be associated with large values of $\tilde{Z}_A|Y \leq h$. Therefore sampling such that we characterise the tail of the distribution of X^* well will likely reduce our uncertainty in estimation of the tail of the distribution of $\tilde{Z}_A|Y \leq h$. We therefore set out deliberately to sample particular values of variables such as X^* more frequently than others; a uniform proposal density is typically suitable. This procedure of course introduces bias, since we deliberately sample in a biased way. It is critical therefore to correct for this bias. The basic methodology for importance sampling can be thought of as follows. First, we choose a proposal distribution (usually denoted by a density “ g ”) which promotes increased sampling of more impactful values relative to sampling from the true or target distribution (usually denoted by density “ f ”) for the variables of interest (which we would employ for simple Monte Carlo sampling). Then we weight the contributions of the sampled points in estimation of $F_{\tilde{Z}_A|Y \leq h}$ to correct for the use of the biased proposal distribution, resulting in an unbiased estimate. Critically, a given precision of estimation can usually be achieved considerably more efficiently when importance sampling is applied well.

We exploit importance sampling multiple times in estimating the cumulative distribution function in Equation 6, as outlined in the steps below. Since we do not have a statistical model for $\{X_s, \Theta_s, \Phi_s, \Omega_s\}|X^*, \Theta^*, \Phi^*$, we adopt a Monte Carlo approach to sample appropriate storm trajectories from a set of historical storm trajectories; the overall approach might therefore be better described as hybrid Monte Carlo-importance sampling. The step-by-step sampling procedure follows Algorithm 1 in broad terms, exploiting importance sampling whenever possible. The procedure is as follows.

Step 1: Sample covariate bin index $d \in \mathcal{I}_d$ uniformly (with proposal density $g_{\mathcal{D}}(d) = 1/n_d$) where $n_d (= |\mathcal{I}_d|)$ is the number of covariate bins covering the full covariate domain \mathcal{P} . Calculate the target density $f_{\mathcal{D}|\mathcal{B}}(d|b)$ for the sampled covariate bin index using the estimated Poisson model for rate $\rho_{\mathcal{D}|\mathcal{B}}(d|b)$ of occurrence of storm peak covariates over directional-seasonal threshold ψ_γ for bootstrap resample b . The proposal-target pair for the importance sampling calculation is therefore

$$g_{\mathcal{D}} = 1/n_d, \quad f_{\mathcal{D}|\mathcal{B}}(d|b) = \frac{\rho_{\mathcal{D}|\mathcal{B}}(d|b)}{\sum_{d' \in \mathcal{I}_d} \rho_{\mathcal{D}|\mathcal{B}}(d'|b)}. \quad (8)$$

The effect of importance sampling at this stage is to increase the rate of sampling from covariate bins with lower storm occurrence rates. This is beneficial from the perspective of characterising extreme environments corresponding to rarer covariate bins, but may be detrimental considering that the most severe events tend to occur from within the most populous covariate bins.

Step 2: Sample the values of storm peak θ^*, ϕ^* uniformly at random from the corresponding covariate bin. This is a simple Monte Carlo sampling step which introduces no bias, for which no importance sampling correction is needed; the proposal-target pair for the corresponding importance sampling calculation are equal.

Step 3: Sample a storm peak value x^* uniformly on a proposal interval $[\psi_\gamma(\theta^*, \phi^*), x_{\max}^+(\theta^*, \phi^*)]$ where $\psi_\gamma(\theta^*, \phi^*)$ is the extreme value threshold for storm peak extreme value modelling for non-exceedance probability γ , and $x_{\max}^+(\theta^*, \phi^*)$ is the finite upper end point for X^* for the covariate bin when it exists, or a pre-specified large quantile of the omni-covariate distribution of return value otherwise. Calculate the target density $f_{X^*|\Theta^*, \Phi^*, \mathcal{B}}(x^*|\theta^*, \phi^*, b)$ using the estimated generalised Pareto extreme value model for size of occurrence of storm peaks. The proposal-target pair for this importance sampling calculation is therefore

$$g_{X^*|\Theta^*, \Phi^*, \mathcal{B}}(x^*|\theta^*, \phi^*, b) = \frac{1}{x_{\max}^+(\theta^*, \phi^*|b) - \psi_\gamma(\theta^*, \phi^*|b)}, \quad f_{X^*|\Theta^*, \Phi^*, \mathcal{B}}(x^*|\theta^*, \phi^*, b) = \text{extreme value model}. \quad (9)$$

The effect of importance sampling at this stage is to increase sampling from the tail of the distribution of $X^*|\Theta^*, \Phi^*, \mathcal{B}$ relative to simple Monte Carlo, which improves the estimation of this region of the distribution.

Step 4: Select and adjust a historical storm trajectory that provides a good empirical match (based on some measure of distance of historical storm peak to sampled θ^*, ϕ^* and x^*). This step provides a time series of $\{x_s, \theta_s, \phi_s, \omega_s\}$ for $s \in \mathcal{S}$, and is identical to that used in Algorithm 1, an unbiased Monte Carlo sampling step, for which no importance sampling correction is needed.

Step 5: Calculate the product $\prod_{s \in \mathcal{S}_i} F_{\tilde{Z}_s|X_s, \Theta_s, \Phi_s, \Omega_s}(z|x_s, \theta_s, \phi_s, \omega_s)^{\mathbb{I}(Y_s \leq h)}$ explicitly over the set \mathcal{S}_i of sea states of

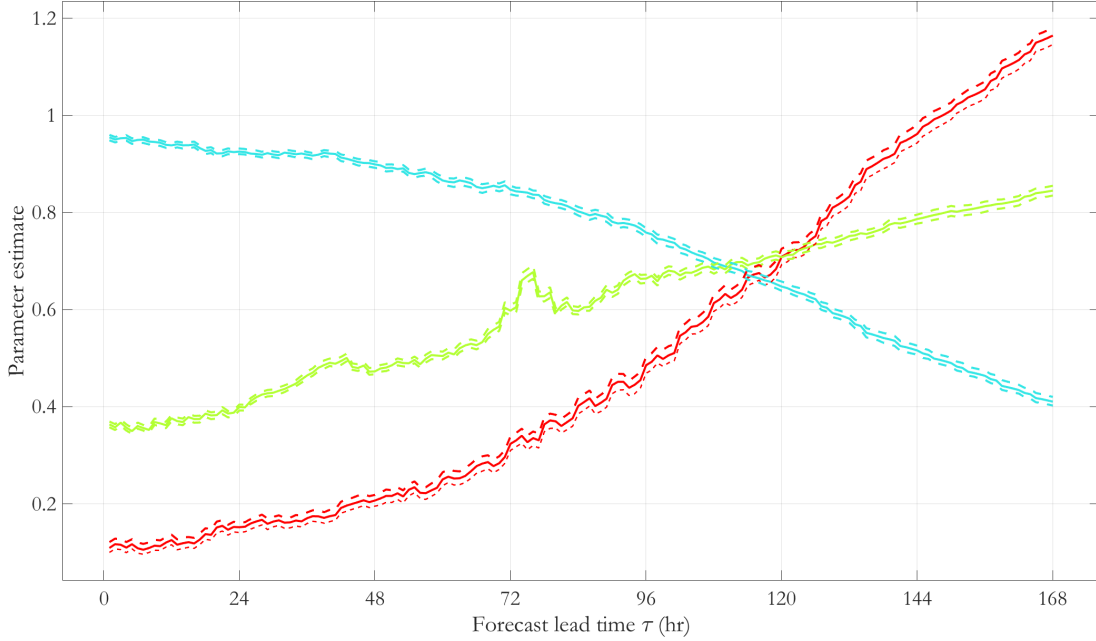


Figure 3: Calibration regression parameter estimates as a function of lead time τ . Intercept $\alpha(\tau)$ (red, m), slope $\beta(\tau)$ (blue, []) and error standard deviation $\sigma(\tau)$ (green, m) estimates shown (solid) with accompanying bootstrap 95% uncertainty bands (dashed). When viewing in greyscale, red, blue and green become dark, medium and light grey respectively.

the storm (now indexed by i for completeness). Finally, calculate the integral in Equation 6 using

$$F_{\tilde{Z}_A|Y \leq h, \mathcal{B}}(z|h, b) = \frac{1}{n_i} \sum_{i=1}^{n_i} \left\{ \left[\prod_{\mathcal{L}_s \in \mathcal{S}_i} F_{\tilde{Z}_s|X_s, \Theta_s, \Phi_s, \Omega_s}(z|x_s, \theta_s, \phi_s, \omega_s)^{\mathbb{I}(Y_s \leq h)} \right] \text{fog}_i(d_i, \theta_i^*, \phi_i^*, x_i^*) \right\} \quad (10)$$

where n_i is the number of storm samples generated, and

$$\text{fog}_i(d_i, \theta_i^*, \phi_i^*, x_i^*) = \frac{f_{\mathcal{D}|\mathcal{B}}(d_i|b) f_{X^*|\Theta^*, \Phi^*, \mathcal{B}}(x_i^*|\theta_i^*, \phi_i^*, b)}{g_{\mathcal{D}}(d_i) g_{X^*|\Theta^*, \Phi^*, \mathcal{B}}(x_i^*|\theta_i^*, \phi_i^*, b)} \quad (11)$$

is the importance sampling likelihood ratio for bias correction for storm i . Once $F_{\tilde{Z}_A|Y \leq h, \mathcal{B}}$ is estimated, optimal un-manning thresholds can be estimated as for simple Monte Carlo using Equations 2 and 6.

4. Un-manning application

In this section, we describe the application of the methodology given in Section 3 to wave impact on a notional structure in the North Sea, using the hindcast and forecast data described in Section 2. Section 4.1 shows results of the weather forecast calibration, and Section 4.2 summarises some of the output of the hierarchical storm model analysis. The main results concerning un-manning threshold estimation are given in Section 4.3. Sections 4.4 outlines a possible operational un-manning alert system. Finally, an assessment of the historical implications of un-manning using the estimated un-manning thresholds is provided in Section 4.5.

4.1. Calibrating the weather forecast

Using the overlapping period of hindcast and forecast data, the calibration model in Equation 7 was estimated. The model estimates forecast H_S for current time t a given lead time τ as a function of the hindcast H_S at time $t + \tau$ as a linear regression, the parameters of which are functions of τ . Parameter estimates with bootstrap 95% uncertainty bands are illustrated in Figure 3. Unsurprisingly, the error standard deviation $\sigma(\tau)$ (green) is estimated to be an increasing function of τ , and the slope parameter $\beta(\tau)$ (blue) a decreasing function. To compensate, the intercept term $\alpha(\tau)$ (red) increases with τ .

Figure 4 illustrates the effect of calibration on four typical samples of time series of sea state H_S . For each panel of the figure, hindcast H_S is shown in blue, and the uncalibrated forecast in red. Corresponding calibrated time-series are shown in green, in terms of a 95% prediction band (thicker lines) and individual calibrated forecast trajectories (thin

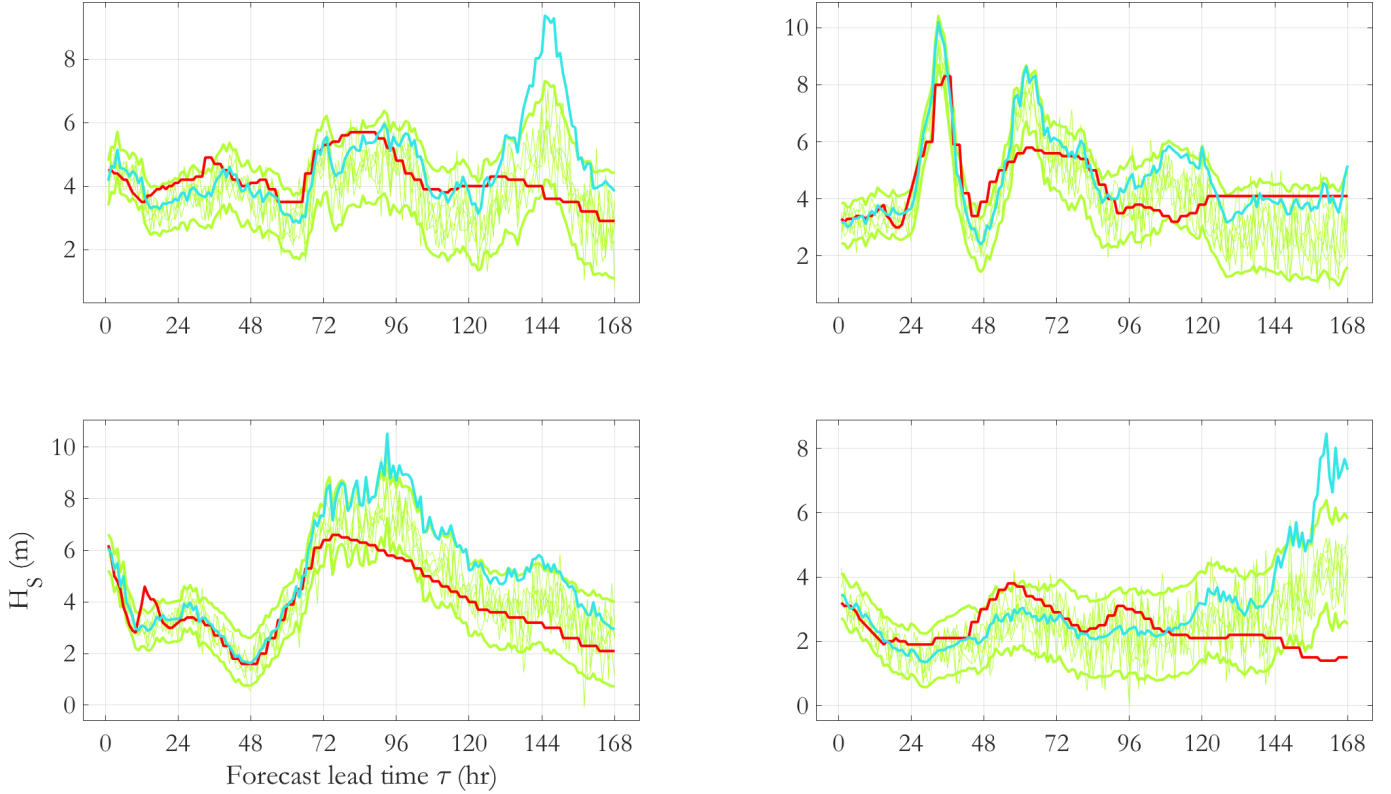


Figure 4: Illustrating forecast calibration. Panels show four examples of intervals of time-series, for which the maximum hindcast H_S exceeds 8m. The hindcast $\{x(t_0 + \tau)\}, \tau \in [0, \tau_{\text{Mxm}}]$ is shown in blue. The corresponding forecast $\{y(\tau; t_0)\}, \tau \in [0, \tau_{\text{Mxm}}]$ made at time t_0 is shown in red. The calibrated forecast $\{y^*(\tau; t_0)\}, \tau \in [0, \tau_{\text{Mxm}}]$ is shown in green in terms of a predictive 95% uncertainty band (bold) and individual realisations (thin) under the fitted model.

lines). Agreement between uncalibrated forecast and hindcast is already good for short lead times τ . The calibration model provides better improves agreement between hindcast and forecast for longer lead times, and quantifies how forecast uncertainty increases with τ .

4.2. Hierarchical model

Details of the hierarchical model are withheld, since the model has been reported a number of times in the literature already. For motivation of the un-manning calculation, however, Figure 5 illustrates the cumulative distribution of maximum total water level, including the effects of waves, tides and surge, for a period of 10^4 years of observation. The solid black line in both left and right panels is the (common) omni-covariate distribution. Other lines in the left panel provide all-year distributions per directional octant. Other lines in the right panel provide omni-directional distributions per month of the year. Not surprisingly for the location under consideration, the directional distribution is dominated by storms from the north, north-west and west; the seasonal distribution is dominated by the winter months.

Intuitively, assuming that the 10^4 year return value is defined as the $\exp(-1) \approx 0.37$ quantile of this distribution, we infer at this location, that structures with deck heights below 21m are at risk from wave-in-deck events. We can also see that un-manning the structure during (e.g.) November would have a material effect on the omni-covariate distribution of maximum total water level restricted to the remaining 11 months.

4.3. Un-manning threshold estimation

Using the estimated hierarchical model, Equations 4 and 5 are used to estimate the $1 - 1/T$ quantile of the annual distribution maximum total water level with $T = 10^4$, restricted to forecast H_S below some threshold h , for each bootstrap resample $b \in \mathcal{B}$. This level could be estimated directly by finding the $1 - 1/T$ quantile of the predictive distribution in Equation 6. However, to minimise bias (see e.g. Jonathan et al. 2021), this level is actually estimated by solving

$$F_{\tilde{Z}_A | Y \leq h, \mathcal{B}}(z_b^*(h) | h, b) = 1 - \frac{1}{T} \quad (12)$$

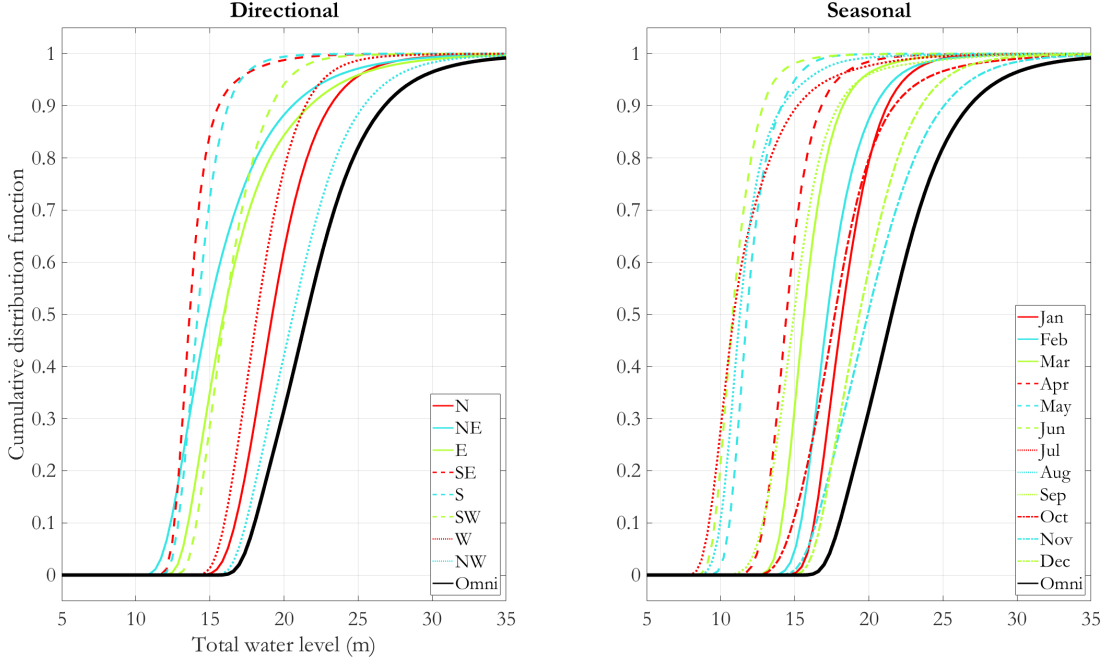


Figure 5: Estimated distribution of the 10,000-year maximum total water level by directional octant (left) and by month (right). Individual lines correspond to estimated distributions for directional or seasonal intervals. Black curves correspond to the (common) “omni” all-season-direction estimate.

per bootstrap resample b , and then averaging the quantile estimates $z_b^*(h)$ over bootstraps so that

$$z^*(h) = \frac{1}{n_b} \sum_{b \in \mathcal{I}_b} z_b^*(h). \quad (13)$$

The resulting estimate $z^*(h)$ is referred to as the T -year mean quantile of total water level, restricted to forecast H_S threshold h . Clearly, this quantile is also conditional on forecast lead time τ : $z^*(h|\tau)$. Estimates for $z^*(h|\tau)$ are shown in the left panel of Figure 6 as a function of h for different forecast lead times τ from 0 hours to 168 hours for $T = 10^4$ years. For a given value of threshold h , the T -year mean quantile level increases with increasing τ due to the increasing uncertainty in forecast H_S . The values of z^* asymptote with increasing h and τ to the $\exp(-1)$ quantile of the “omni” all-season-direction quantile of the distribution of the 10^4 -year maximum shown in black in Figure 5.

The right panel of Figure 6 gives the resulting un-manning threshold h^* obtained by solving

$$z^*(h^*(\tau|d)|\tau) = d \quad (14)$$

for deck height d . The figure shows $h^*(\tau|d)$ for 7 different choices of deck height.

The lowest 5 deck heights are included to illustrate the behaviour of h^* with τ and d for h^* levels which are encountered multiple times during the period \mathcal{I}_{Hnd} of the hindcast. The highest level $d = 20\text{m}$ is a more realistic value for a notional structure at the location under consideration, since this corresponds approximately to the asymptote in the left panel of the figure.

4.4. A notional alert system

With a deck height of 16m, Figure 6 suggests that un-manning at a forecast lead time of $\tau = 100$ hours would be necessary when forecast H_S exceeds 8m. At 160 hours, the corresponding un-manning threshold reduces to approximately 5m. Figure 7 shows a notional alert system that might be adopted operationally, with action thresholds shown for hypothetical deck height $d = 16\text{m}$ (solid curve) and an alert deck height of 12m (dashed curve).

The alert system proposed is multi-tiered: if forecast H_S falls in the green area of the figure, no action is required. However, if the forecast H_S falls into either the grey or red areas, an un-manning alert would be issued for preparation of execution of un-manning respectively. For the illustration in Figure 7, there are two instances of forecast H_S entering the grey area. For one instance, forecast H_S exceeds the un-manning thresholds for $\tau > 100$ hours for both the full and alert deck heights. For this lead time, it is probably feasible to un-man the facility safely. However, the second instance corresponds to an exceedance of the alert level at lead time of $\tau = 24$ hours. Depending on the circumstances,

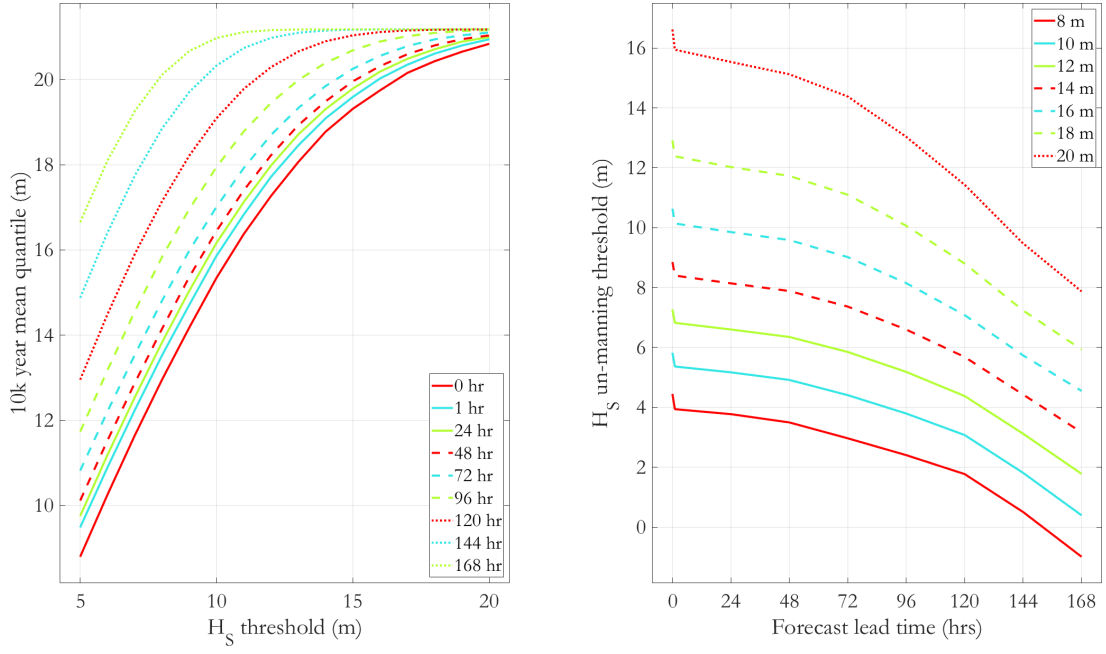


Figure 6: Illustration of un-manning curves. The left hand panel shows bootstrap mean effective “manned” 10,000-year return value $z^*(h|\tau)$ for total water level as a function of h , the un-manning threshold H_S , for different lead times τ . The right hand panel shows the resulting un-manning threshold $h^*(\tau|d)$ as a function of τ for assumed deck heights $d = 8, 10, \dots, 20\text{m}$. Line colours and styles in the right hand panel are also used in Figure 8 for ease of comparison.

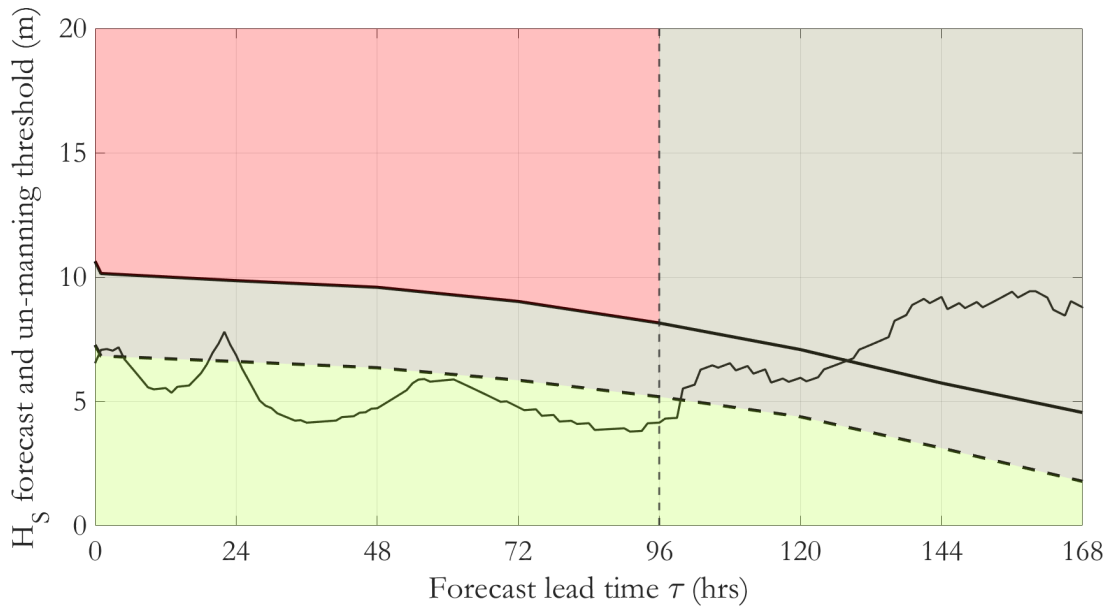


Figure 7: Illustration of a notional alert system. Alert threshold as a function of lead time τ shown in dashed black. Action threshold shown in solid black. Forecast H_S shown in solid black. Coloured zones represent lead times at which forecast exceedances of thresholds are viewed as “for preparation” (grey) and “for action” (red). Vertical black line represents critical lead time (the largest value of τ for which immediate action is not required).

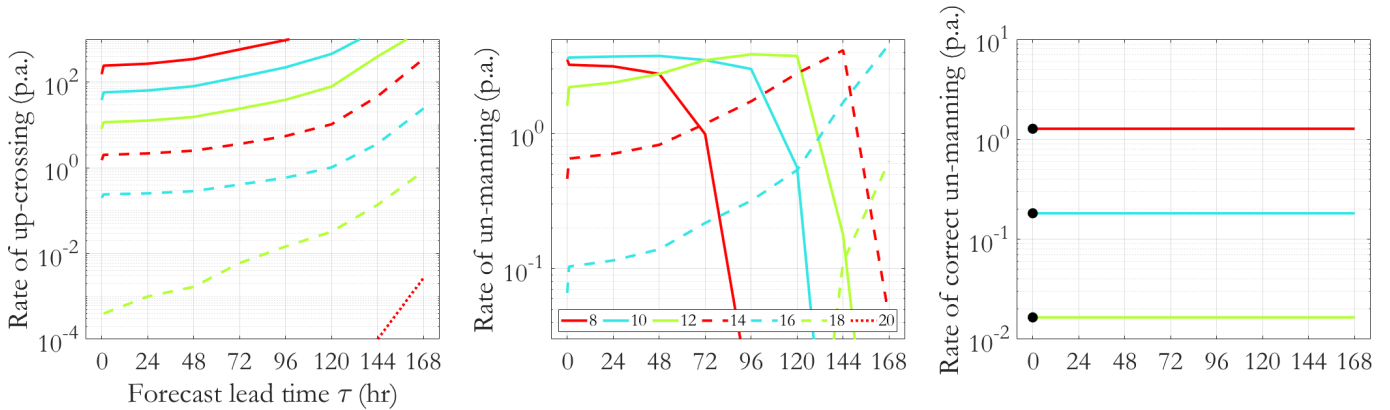


Figure 8: Illustration of historical performance of action strategy. Left: Historical annual rates of occurrence of individual exceedances of un-manning threshold as a function of lead time τ for deck heights $d = 8, 10, \dots, 20$ m. Centre: Historical annual rate of triggered un-manning events. Right: Historical annual rate of correctly-triggered un-manning events for $d = 8, 10, 12$ m. The corresponding actual rate of wave in deck is indicated by black discs at $\tau = 0$. The legend relevant for all panels is given in the centre panel; the line labelling scheme is the same as that used in the right panel of Figure 6. The return period (in years) of a particular event is simply the reciprocal of the corresponding annual rate.

shut-down or (partial) un-manning might be deemed necessary. It is clear that if forecast H_S for small τ occurs within the red area, then full un-manning might not be feasible, emphasising the importance of high-quality H_S forecasts for lead times up to 5 days, and minimising the number of such occurrences.

4.5. Outline of historical performance of alert system

Using the 61 years of hindcast data and the calibration model from Equation 7, it is possible to identify occurrences of historical un-manning for the notional North Sea structure. We assume for illustration that un-manning is triggered when the forecast H_S for some lead time τ exceeds the un-manning threshold h^* illustrated in Figure 6. Further, an un-manning event here is assumed to require the facility to be un-manned for at least one week. Hence, subsequent exceedances of the un-manning threshold within an existing un-manning period are assumed therefore not to trigger further un-manning. Results for different deck heights d (lines) and forecast lead times τ are given in Figure 8.

The left panel of Figure 8 illustrates the annual rate of forecast occurrence of individual (sea state) up-crossings of the un-manning threshold. As expected, the rate of up-crossings increases with decreasing deck height. The centre panel indicates the annual rate of triggered un-manning events as a function of d and τ . For deck height $d = 8, 10, 12$ m, this rate is of the order of 2 to 4. For $d = 14$ m (16m), the rate of un-manning increases from approximately 0.1 (0.7) (at $\tau = 0$) to 4 (for large τ). At $d = 18$ m, un-manning would only be considered for large τ , and in reality probably not triggered because of the large value of τ . There are no historical triggered un-manning events for $d = 20$ m. The rates of triggered un-manning events are clearly lower than those for up-crossings of un-manning threshold.

The right panel shows the annual rate of correctly-detected wave in deck events for $d = 8, 10, 12$ m. The corresponding actual rate of wave in deck is indicated by the black discs at $\tau = 0$. All observed wave in deck events trigger un-manning events based on the forecast, for all values of τ . The reason for this is that the un-manning threshold has been estimated using the procedure described in Sections 3 and 4 for this specific forecast model, for each value of τ of interest. For a relatively poor forecast model, the un-manning threshold for a given τ will be lower than for a better forecast model. As a result, the rate of unnecessary (of ‘false positive’) un-manning will be higher for poorer forecast models. For instance, referring to right hand panel of Figure 6, the un-manning threshold for $\tau = 24$ hr and a deck height of 16m corresponds to approximately 10m. Using the current forecast model, it is extremely unlikely that an actual occurrence of wave in deck (i.e. true $H_S > 16$ m) would correspond to a calibrated forecast $H_S < 10$ m: hence all actual wave in deck events trigger un-manning based on the forecast. However, the forecast also triggers a relatively large number of undesirable ‘false positive’ un-manning events. Clearly, as the quality of the forecast improves, the un-manning threshold for a given τ will increase, and the rate of unnecessary un-manning will reduce ultimately to zero.

5. Discussion and conclusions

In this article we present a computationally efficient approach to estimation of extreme ocean environments, illustrated by application to construction of an un-manning strategy for a notional North Sea structure. The approach exploits a hierarchical model for the ocean environment to estimate the tail of the distribution of annual maximum total water

level. The un-manning strategy is premised on our ability to remove personnel from the structure during the severest conditions, so that the reliability of the structure whilst manned is acceptable. The computational efficiency of the approach is achieved by judicious use of importance sampling in place of Monte Carlo sampling in the evaluation of multidimensional integrals.

Wave in deck is the focus of the current work, and hence maximum total water level the “response” variable of concern. However, the un-manning approach presented here (described by Equation 4) is applicable generally to any structural response Z of interest. The computational tools described have also been applied successfully to the direct estimation of Morison-type loading and hence probability of failure, utilisation, etc. for full-scale structural models. There is cause for concern that too much modelling effort is dedicated to the estimation of environmental return values, as opposed to thorough quantification of probability of structural failure subject to an uncertain ocean environment (Serinaldi 2015, Jonathan et al. 2021).

An alternative approach to un-manning is to trigger an un-manning event when the characteristics of an individual severe storm are such that the probability of wave in deck (or some other extreme structural response) exceeds some threshold. The difficulty with this approach is the decision to un-man does not guarantee a given level of structural reliability per annum, unless the rate of occurrence of the severe storm is also incorporated in the decision-making procedure. Hagen and Solland (2009) and NORSOK N-006 (2015) argue for a composite approach, with extra conditions on individual forecast events which do not trigger un-manning based on annual criteria. Hence, individual extreme forecasted storms may also trigger un-manning.

Establishing an effective operational procedure for un-manning an offshore structure is a complex task. In the current work, we have only considered risk reduction from the perspective of reducing the exposure time of personnel to the most extreme environments to an acceptable level. However, the decision to un-man a structure incurs other risks to personnel (e.g. from helicopter flights in severe conditions). In addition, it is likely that the severest storms will trigger un-manning events at multiple platforms, placing constraints on resources; experiences from hurricane and cyclone-dominated regions including the Gulf of Mexico and South China Sea provide useful guidance. The computational tools discussed in this article provide some of the methodology required to optimise the un-manning procedure.

6. Acknowledgements

The authors gratefully acknowledge DTN (2021) for the provision of forecast data and their general support for this publication, and useful discussions with Emmanuel Fakas (Shell, Aberdeen) and Oliver Jones (BP, London). We also thank two reviewers for comments on the manuscript.

References

- Davison, A.C., 2003. *Statistical models*. Cambridge University Press, Cambridge, UK.
- DNVGL-RP-C205, 2017. *Environmental conditions and environmental loads*. Det Norske Veritas group, Norway.
- DTN, 2021. www.dtn.com.
- Ewans, K.C., Jonathan, P., 2008. The effect of directionality on northern North Sea extreme wave design criteria. *J. Offshore. Arct. Eng.* 130, 041604:1–041604:8.
- Feld, G., Randell, D., Jonathan, P., 2019. On the estimation and application of directional design criteria. *Proc. 38th Int. Conf. on Ocean, Offshore & Arctic Engineering*, Scotland .
- Feld, G., Randell, D., Wu, Y., Ewans, K., Jonathan, P., 2015. Estimation of storm peak and intra-storm directional-seasonal design conditions in the North Sea. *J. Offshore. Arct. Eng.* 137, 021102:1–021102:15.
- Forristall, G.Z., 2000. Wave crest distributions: Observations and second-order theory. *J. Phys. Oceanogr.* 30, 1931–1943.
- Gelfand, A.E., 1994. Model determination using sampling-based methods. Edts. W. R. Gilks, S. Richardson and D. S. Spiegelhalter, London: Chapman and Hall. pp. 144–161.
- Hagen, O., Riise, B., 2012. OMAE2012-83648: Ensemble forecasts used for extreme wave warning and platform un-manning strategies. *Proc. 31st Conf. Offshore Mech. Arct. Eng.* .
- Hagen, O., Solland, G., 2009. Extreme weather warning criteria. *International Conference on Offshore Mechanics and Arctic Engineering. V2: Structures, Safety and Reliability* , 757–763.

- Hagen, O., Solland, G., 2013. OMAE2013-11480: On safety and reliability for platforms that are unmanned during severe storms. Proc. 32st Conf. Offshore Mech. Arct. Eng. .
- ISO19901-1, 2015. Petroleum and natural gas industries. Specific requirements for offshore structures. Part 1: Metocean design and operating considerations. First edition. International Standards Organisation.
- Jonathan, P., Randell, D., Wadsworth, J., Tawn, J., 2021. Uncertainties in return values from extreme value analysis of peaks over threshold using the generalised Pareto distribution. *Ocean Eng.* 220, 107725.
- Jones, M.J., Hansen, H.F., Zeeberg, A.R., Randell, D., Jonathan, P., 2018. Uncertainty quantification in estimation of ocean environmental return values. *Coastal Eng.* 141, 36–51.
- Karmpadakis, I., Swan, C., Christou, M., 2019. Laboratory investigation of crest height statistics in intermediate water depths. *Proceedings of the Royal Society A: Mathematical, Physical and Engineering Sciences* 475, 20190183.
- Karmpadakis, I., Swan, C., Christou, M., 2020. Assessment of wave height distributions using an extensive field database. *Coastal Eng.* , 103630.
- Meucci, A., Young, I.R., Hemer, M., Kirezci, E., Ranasinghe, R., 2020. Projected 21st century changes in extreme wind-wave events. *Science Advances* 6, 1–10.
- NORSOK N-006, 2015. NORSOK Standard N-006:2015: Assessment of structural integrity for existing offshore load-bearing structures. NORSOK, Norway.
- Northrop, P., Attalides, N., Jonathan, P., 2017. Cross-validators extreme value threshold selection and uncertainty with application to ocean storm severity. *J. Roy. Statist. Soc. C* 66, 93–120.
- Randell, D., Feld, G., Ewans, K., Jonathan, P., 2015. Distributions of return values for ocean wave characteristics in the South China Sea using directional-seasonal extreme value analysis. *Environmetrics* 26, 442–450.
- Reistad, M., Breivik, O., Haakenstad, H., Aarnes, O.J., Furevik, B.R., Bidlot, J.R., 2011. A high-resolution hindcast of wind and waves for the North Sea, the Norwegian Sea, and the Barents Sea. *J. Geophys. Res.* 116, 1–18.
- Schubert, M., Wu, Y., Tychsen, J., Faber, M.H., Sorensen, J.D., Jonathan, P., 2020. On the distribution of maximum wave and crest height at intermediate water depths. *Ocean Eng.* 217, 107485.
- Serinaldi, F., 2015. Dismissing return periods! *Stoch. Env. Res. Risk A.* 29, 1179–1189.
- Tendijck, S., Ross, E., Randell, D., Jonathan, P., 2019. A non-stationary statistical model for the evolution of extreme storm events. *Environmetrics* 30, e2541.
- Zanini, E., Eastoe, E., Jones, M., Randell, D., Jonathan, P., 2020. Covariate representations for non-stationary extremes. *Environmetrics* 31, e2624.